IEEE Access
Multidisciplinary | Rapid Review | Open Access Journal

Received January 28, 2020, accepted February 11, 2020, date of publication February 20, 2020, date of current version February 27, 2020.

Digital Object Identifier 10.1109/ACCESS.2020.2974753

An Integration-Implemented Newton-Raphson Iterated Algorithm With Noise Suppression for Finding the Solution of Dynamic Sylvester Equation

GUANCHENG WANG[1,2], HAOEN HUANG[1,2], JINGKUN YAN[3], YIHANG CHENG[1,2], AND DONGYANG FU[1,2]

[1]School of Electronics and Information Engineering, Guangdong Ocean University, Zhanjiang 524025, China
[2]Shenzhen Institute, Guangdong Ocean University, Shenzhen 518108, China
[3]School of Information Science and Engineering, Lanzhou University, Lanzhou 730000, China

Corresponding author: Dongyang Fu (fdy163@163.com)

This work was supported in part by the Fund of Southern Marine Science and Engineering Guangdong Laboratory, Zhanjiang, under Grant ZJW-2019-08, in part by the Project of Enhancing School with Innovation of Guangdong Ocean University under Grant GDOU2014050226, in part by the Project of Innovation Training Project of Guangdong Ocean University under Grant CXXL2019276, and in part by the Innovation and Strength Project of Guangdong Ocean University under Grant Q15090 and Grant 230419065.

ABSTRACT Solving dynamic Sylvester matrix equations is a prevalent research topic and many methods have been arisen to solve the dynamic Sylvester equation, but few of them consider the noise effect. To investigate the new approach which can suppress the noise effect, integration feedback is added in the conventional Newton-Raphson iterated (CNRI) algorithm to form the proposed integration-implemented Newton-Raphson iterated (IINRI) algorithm based on the control theorem. Besides, this paper transforms the dynamic Sylvester equation into a linear equation which turns into the zeroing finding problem in further by constructing the error function. According to the theoretical analyses and the simulation results, the IINRI algorithm has higher accuracy and strong robustness under different noises (e.g. the constant noise, the linear noise, and the bounded random noise) while the performance of the CNRI algorithm is seriously degraded by the noises, which reveals that the IINRI algorithm is an efficient and powerful approach to solve dynamic Sylvester equation under noise perturbations.

INDEX TERMS Dynamic Sylvester equation, integration-implemented, Newton-Raphson iterated algorithm, noise suppression.

I. INTRODUCTION

Finding the solution of dynamic Sylvester equation plays a crucial role in many fields, such as in control system [1]–[3], image processing [4]–[7], and stability analysis [8]. Thus, many efficient approaches are presented to solve the dynamic Sylvester equation in the last decades, mainly including iterative algorithms [9]–[14] and recurrent neural network models [15]–[21]. For example, Xie and Ma divide the Sylvester-transpose matrix equation into two subsystems and derive the iterated algorithm based on least-squares optimization [11]. Regarding the recurrent neural network, it is very popular in recent years and has been exploited as a solution to a variety of problems [22]–[26]. Liao *et al.* introduce an adaptive parameter gradient neural network (GNN) with avoiding the matrix inverse [15]. Furthermore, a modified zeroing neural network (ZNN) model is presented with shorter convergence time [20]. Generally speaking, the ZNN model can utilize the time-derivation information of coefficients to obtain the theoretical solution to dynamic problems, while the cost is to possess higher computing complexity. Besides, it is worth pointing out that the derivation term is extremely susceptible to noise perturbations. Therefore, the above-mentioned algorithms are deemed isolated from noises during the calculation process, which limits their applications in the practical workspace.

Noises widely occur in the computing system, which may degrade the accuracy of computing solution or even cause the

The associate editor coordinating the review of this manuscript and approving it for publication was Okyay Kaynak.

algorithm to fail. For example, the ZNN model can find the theoretical solution without the noises while it would diverge under the linear noise perturbation [27], [28]. Though many techniques have been exploited to suppress noises, such as calibration algorithm, filter, and others [29]–[33], noise is still inevitable in the system. For example, the truncation error, the rounding error, and the offset error can be seen as the noise perturbation. Thus, suppressing noises from the perspective of the algorithm property is of great necessity and significance. Though few methods can suppress noises based on numerical theory, there are many mature approaches to cope with various noises in control theorem. In the light of control theory, the Newton-Raphson iteration algorithm can be deemed as a proportional feedback system [34], [35]. Besides, it is acknowledged that an integration feedback term can effectively suppress noises. Therefore, motivated by that conception, an integration-implemented Newton-Raphson iterated (IINRI) algorithm with low computing complexity is proposed in this paper.

The rest of this paper is divided into four sections. The derivation and formulation of the IINRI algorithm for solving the dynamic Sylvester equation are introduced in Section II. For comparison, the conventional Newton-Raphson iterated (CNRI) algorithm is also presented in this section. Section III investigates the accuracy and convergence of the IINRI algorithm, especially under various noisy environments. Theoretical analyses demonstrate the superiority of the IINRI algorithm on noise suppression and provide a strategy to improve the accuracy versus various types of noises. For illustration, simulation results are presented in Section IV, which well verify the correctness of the corresponding theoretical analyses aforementioned. Finally, Section V concludes this paper. At the end of this section, the highlights of this paper are summarized below.

1) This paper proposes an IINRI algorithm derived from the CNRI algorithm, improving the accuracy from $O(\tau)$ to $O(\tau^2)$.
2) In the presence of various types of noises, the IINRI reveals its strong robustness and high accuracy. Especially, under the constant-noise workspace, the IINRI algorithm still keeps the excellent performance as the same as in the case of the noise-free workspace no matter how large the constant noise is.
3) Theoretical analyses and numerical simulations are provided to prove and verify the superiority of the IINRI algorithm.

II. PROBLEM AND THE PROPOSED IINRI ALGORITHM

At the beginning of this section, the dynamic Sylvester equation is introduced. Then, the IINRI algorithm derived from the CNRI algorithm is proposed, which is implemented with an integration item for suppressing noises.

A. DYNAMIC SYLVESTER EQUATION

The dynamic Sylvester equation can be formulated as

$$M(t)Z(t) - Z(t)N(t) + L(t) = 0, \tag{1}$$

with parameter matrixes $M(t) \in \mathbb{R}^{m\times m}$, $N(t) \in \mathbb{R}^{n\times n}$, and $L(t) \in \mathbb{R}^{m\times n}$. The major task of this paper is to find the unknown matrix $Z(t) \in \mathbb{R}^{m\times n}$, making it infinitely close to the theoretical $Z^*(t)$.

For monitoring and controlling the solving process, an error function is constructed as:

$$E\big(Z(t)\big) = M(t)Z(t) - Z(t)N(t) + L(t), \tag{2}$$

where $E\big(Z(t)\big) \in \mathbb{R}^{m\times n}$. According to the Kronecker product theory, we have

$$\mathrm{vec}(AYB) = (B^{\mathrm{T}} \otimes A)\mathrm{vec}(Y),$$

where A, B, and Y are matrixes. Besides, $\mathrm{vec}(\cdot)$ symbolizes the vectorization operation, and $\otimes$ stands for the Kronecker product. Thus, $E\big(Z(t)\big)$ can be vectorized as

$$\boldsymbol{e}(t) = \big(\boldsymbol{I}_n \otimes M(t)\big)\boldsymbol{z}(t) - \big(N^{\mathrm{T}}(t) \otimes I_m\big)\boldsymbol{z}(t) - \boldsymbol{l}(t), \tag{3}$$

where I_n and I_m are unit matrixes of size n^2 and m^2, respectively. Moreover, $\boldsymbol{e}(t) \in \mathbb{R}^{mn}$, $\boldsymbol{z}(t) \in \mathbb{R}^{mn}$, and $\boldsymbol{l}(t) \in \mathbb{R}^{mn}$ denote the vectorization of $E\big(Z(t)\big)$, $Z(t)$, and $L(t)$, respectively. For simplicity, (3) can be rewritten as

$$\boldsymbol{e}(t) = A(t)\boldsymbol{z}(t) - \boldsymbol{l}(t), \tag{4}$$

with $A(t) = \big(\boldsymbol{I}_n \otimes M(t)\big) - \big(N^{\mathrm{T}}(t) \otimes I_m\big) \in \mathbb{R}^{mn\times mn}$.

B. PROPOSED IINRI ALGORITHM

Sampling the system at time instant $t = k\tau$ with τ denoting the sampling interval, a discrete-time form of (4) can be obtained as

$$\boldsymbol{e}_k = A_k\boldsymbol{z}_k - \boldsymbol{l}_k. \tag{5}$$

Thus the CNRI algorithm for solving (5) can be expressed as

$$\boldsymbol{x}_{k+1} = \boldsymbol{x}_k - A_k^{-1}\boldsymbol{e}_k. \tag{6}$$

Subsequently, (6) can be rearranged as

$$A_k\frac{\boldsymbol{x}_{k+1} - \boldsymbol{x}_k}{\tau} = -\frac{1}{\tau}\boldsymbol{e}_k = \dot{\boldsymbol{e}}_k, \tag{7}$$

where $\dot{\boldsymbol{e}}_k$ is the time derivative of $\boldsymbol{e}_k$. For the purpose of suppressing noises, an integration item is added in (7), which can be formulated as

$$\dot{\boldsymbol{e}}_k = -\frac{1}{\tau}\boldsymbol{e}_k - \alpha\tau\sum_{i=0}^{k}\boldsymbol{e}_i, \tag{8}$$

of which $\alpha > 0$ is a scale factor. Combining (7) and (8), the IINRI algorithm is proposed as

$$\boldsymbol{x}_{k+1} = \boldsymbol{x}_k - A_k^{-1}(\boldsymbol{e}_k + \alpha\tau^2\sum_{i=0}^{k}\boldsymbol{e}_i). \tag{9}$$

III. THEORETICAL ANALYSES

In this section, the accuracy and convergence of the IINRI algorithm (9) are analyzed. Besides, the performances of the IINRI algorithm (9) under different noisy environments are investigated. Before these analyses, an equivalent expression of the IINRI algorithm (9) is presented as below. Polluted by the noise perturbation $\boldsymbol{\epsilon} \in \mathbb{R}^{mn}$, (8) can be expressed as

$$\dot{\boldsymbol{e}}_k = -\frac{1}{\tau}\boldsymbol{e}_k - \alpha\tau\sum_{i=0}^{k}\boldsymbol{e}_i - \boldsymbol{\epsilon}. \tag{10}$$

Correspondingly, the IINRI algorithm (9) can be rewritten as

$$\boldsymbol{x}_{k+1} = \boldsymbol{x}_k - A_k^{-1}(\boldsymbol{e}_k + \alpha\tau^2\sum_{i=0}^{k}\boldsymbol{e}_i + \tau\boldsymbol{\epsilon}). \tag{11}$$

In the light of Taylor expansion, the expansion formulation of (10) with respect to $\dot{\boldsymbol{e}}_k$ can be expressed as

$$\boldsymbol{e}_k + \tau\dot{\boldsymbol{e}}_k + \alpha\tau^2\sum_{i=0}^{k}\boldsymbol{e}_i + \tau\boldsymbol{\epsilon} + \boldsymbol{O}(\tau^2) = \boldsymbol{0}. \tag{12}$$

Expanding $\dot{\boldsymbol{e}}_k$ as

$$\dot{\boldsymbol{e}}_k = \frac{\boldsymbol{e}_{k+1} - \boldsymbol{e}_k}{\tau}, \tag{13}$$

(12) can be rewritten as

$$\boldsymbol{e}_{k+1} + \alpha\tau^2\sum_{i=0}^{k}\boldsymbol{e}_i + \boldsymbol{O}(\tau^2) + \tau\boldsymbol{\epsilon} = \boldsymbol{0}. \tag{14}$$

A. NOMINAL CONVERGENCE

To investigate the convergence and accuracy of the IINRI algorithm (9), the following theorem is provided.

Theorem 1: Finding the solution of dynamic Sylvester equation with the IINRI algorithm (9), the Euclidean norm of error $||\boldsymbol{e}||_2$ converges to $O(\tau^2)$ when $0 < \alpha\tau^2 < 1$.

Proof: The j^{th} subsystem of (14) without the noise $\boldsymbol{\epsilon}$ at the $(k+1)^{\text{th}}$ time interval can be expressed as

$$\boldsymbol{e}_{k+1}^j + \alpha\tau^2\sum_{i=0}^{k}\boldsymbol{e}_i^j + O(\tau^2) = 0. \tag{15}$$

Similarly, the j^{th} subsystem of (14) without the noise $\boldsymbol{\epsilon}$ at the k^{th} time interval can be expressed as

$$\boldsymbol{e}_k^j + \alpha\tau^2\sum_{i=0}^{k-1}\boldsymbol{e}_i^j + O(\tau^2) = 0. \tag{16}$$

Then, subtracting (15) by (16) could yield

$$\boldsymbol{e}_{k+1}^j = \beta\boldsymbol{e}_i^j + O(\tau^2), \tag{17}$$

where $\beta = 1 - \alpha\tau^2$. Based on (17), the relationship between $\boldsymbol{e}_{k+1}$ and $\boldsymbol{e}_0$ can be evolved as

$$\begin{aligned}\boldsymbol{e}_{k+1}^j &= \beta\boldsymbol{e}_k^j + O(\tau^2)\\ &= \beta\big(\beta\boldsymbol{e}_{k-1}^j + O(\tau^2)\big) + O(\tau^2)\\ &= \beta^2\boldsymbol{e}_{k-1}^j + \beta O(\tau^2) + O(\tau^2)\\ &= \beta^2\boldsymbol{e}_{k-1}^j + O(\tau^2)\\ &\;\;\vdots\\ &= \beta^{k+1}\boldsymbol{e}_0^j + O(\tau^2).\end{aligned}$$

If $0 < \beta < 1$, i.e., $0 < \alpha\tau^2 < 1$, it has

$$\lim_{k\to\infty}\boldsymbol{e}_{k+1}^j = \lim_{k\to\infty}\beta^{k+1}\boldsymbol{e}_0^j + O(\tau^2) = O(\tau^2). \tag{18}$$

Thus,

$$\lim_{k\to\infty}||\boldsymbol{e}_{k+1}||_2 = O(\tau^2). \tag{19}$$

The proof is thus complete. □

From above analyses, solving the dynamic Sylvester equation by the IINRI algorithm (9), the initial state $\boldsymbol{x}_0$ converges to the theoretical solution with residual error $O(\tau^2)$. Moreover, compared with the the CNRI algorithm (6) whose accuracy is $O(\tau)$ [36], the IINRI algorithm (9) can improve the accuracy to $O(\tau^2)$.

B. THE ROBUSTNESS AGAINST CONSTANT NOISES

The constant noise, the offset, and the mean of random noise are usually encountered in industry production. To investigate the performance of the IINRI algorithm (9) under the constant-noise perturbation, the following theorem is provided.

Theorem2: Solving the dynamic Sylvester equation by the IINRI algorithm (9) under the constant noise $\boldsymbol{\epsilon}$, the Euclidean norm of error $||\boldsymbol{e}||_2$ converges to $O(\tau^2)$.

Proof: The IINRI algorithm (9) perturbed by the constant noise $\boldsymbol{\epsilon}$ can be formulated as

$$\boldsymbol{e}_{k+1} + \alpha\tau^2\sum_{i=0}^{k}\boldsymbol{e}_i + \boldsymbol{O}(\tau^2) + \tau\boldsymbol{\epsilon} = \boldsymbol{0}. \tag{20}$$

Similar to the Proof of Theorem 1, the difference between the expression at the $(k+1)^{th}$ and the k^{th} time interval of the j^{th} subsystem of (20) can be expressed as

$$\boldsymbol{e}_{k+1}^j = \beta\boldsymbol{e}_i^j + O(\tau^2), \tag{21}$$

which is the same as (17). Thus, the proof is omitted and completed. □

It is necessary to emphasis that the steady-state residual error of the IINRI algorithm (9) is independent of the constant noise. That is to say, no matter how large the constant noise is, the accuracy of the IINRI algorithm (9) always is $O(\tau^2)$.

C. THE ROBUSTNESS AGAINST LINEAR NOISES

To demonstrate the robustness of the IINRI algorithm (9) against the linear noise, the following theorem is provided.

Theorem3: Solving the dynamic Sylvester equation by the IINRI algorithm (9) with the linear noise $\boldsymbol{\epsilon}_k = k\tau\boldsymbol{\gamma} + \boldsymbol{\omega}$, where $\boldsymbol{\gamma} \in \mathbb{R}^{mn}$ and $\boldsymbol{\omega} \in \mathbb{R}^{mn}$ are independent

of time, the Euclidean norm of error $||\boldsymbol{e}||_2$ converges to $||\boldsymbol{\gamma}||_2/\alpha + O(\tau^2)$.

Proof: The IINRI algorithm (9) perturbed by the linear noise $k\tau\boldsymbol{\gamma}$ can be formulated as

$$\boldsymbol{e}_{k+1} + \alpha\tau^2 \sum_{i=0}^{k} \boldsymbol{e}_i + \boldsymbol{O}(\tau^2) + \tau^2\boldsymbol{\gamma}k = \boldsymbol{0}. \tag{22}$$

Regarding to the linear noise, formula (17) turns into

$$\boldsymbol{e}_{k+1}^j = \beta\boldsymbol{e}_i^j + O(\tau^2) + \tau^2\boldsymbol{\gamma}^j. \tag{23}$$

Then doing the backward iteration, $\boldsymbol{e}_{k+1}^j$ can be approximated as

$$\begin{aligned}
\boldsymbol{e}_{k+1}^j &= \beta\boldsymbol{e}_k^j + \tau^2\boldsymbol{\gamma}^j + O(\tau^2) \\
&= \beta^2\boldsymbol{e}_{k-1}^j + \tau^2\boldsymbol{\gamma}^j(1+\beta) + O(\tau^2) \\
&\;\;\vdots \\
&= \beta^{k+1}\boldsymbol{e}_0^j + \tau^2\boldsymbol{\gamma}^j(1+\beta+\ldots+\beta^k) + O(\tau^2). \\
&= \beta^{k+1}\boldsymbol{e}_0^j + \tau^2\boldsymbol{\gamma}^j\frac{1-\beta^k}{1-\beta} + O(\tau^2).
\end{aligned}$$

Therefore, when $k \to \infty$, it has

$$\lim_{k\to\infty} \boldsymbol{e}_{k+1} = \frac{\boldsymbol{\gamma}^j}{\alpha} + O(\tau^2). \tag{24}$$

Obviously, the steady-state residual error generated by the IINRI algorithm (9) with the linear noise is $||\boldsymbol{\gamma}||_2/\alpha + O(\tau^2)$. The proof is thus completed. □

Fortunately, for that linear noises, the high accuracy of the IINRI algorithm (9) can be guaranteed by enlarging the scale factor α. Besides, in the case of $\boldsymbol{\gamma} = \boldsymbol{0}$, the linear noise can be deemed as the constant noise and the accuracy is approximately $O(\tau^2)$, which verifies the correctness of Theorem 2.

D. THE ROBUSTNESS AGAINST BOUNDED RANDOM NOISES

Regarding to the case perturbed by the bounded random noises, the following theorem is provided. *Theorem4:* Solving the dynamic Sylvester equation with the IINRI algorithm (9) polluted by the bounded random noise $\boldsymbol{\epsilon}_k \in (-\boldsymbol{\epsilon_m}, \boldsymbol{\epsilon_m})$ where $\boldsymbol{\epsilon_m}$ is the boundary of the random noise, the Euclidean norm of error $||\boldsymbol{e}||_2$ is with the boundary $||\boldsymbol{\epsilon}_m||_2/\alpha\tau + O(\tau^2)$.

Proof: From (14), the IINRI algorithm (9) perturbed by the bounded random noise can be expressed as

$$\boldsymbol{e}_{k+1} + \alpha\tau^2 \sum_{i=0}^{k} \boldsymbol{e}_i + \mathbf{O}(\tau^2) + \boldsymbol{\epsilon}_k = \boldsymbol{0}, \tag{25}$$

Similarly, (25) can be rewritten as

$$\boldsymbol{e}_{k+1}^j = \beta\boldsymbol{e}_k^j + \tau\triangle\boldsymbol{\epsilon}_k^j + O(\tau^2), \tag{26}$$

where $\triangle\boldsymbol{\epsilon}_k^j = \boldsymbol{\epsilon}_k^j - \boldsymbol{\epsilon}_{k-1}^j (k \geq 1)$. Besides, according to (25),

$$\boldsymbol{e}_1 + \alpha\tau^2\boldsymbol{e}_0 + \mathbf{O}(\tau^2) + \boldsymbol{\epsilon}_0 = \boldsymbol{0}. \tag{27}$$

Thus, doing backward iteration based on (26) and (27) leads to

$$\begin{aligned}
\boldsymbol{e}_{k+1}^j &= \beta\boldsymbol{e}_k^j + \tau\triangle\boldsymbol{\epsilon}_k^j + O(\tau^2) \\
&= \beta\big(\beta\boldsymbol{e}_{k-1}^j + \tau\triangle\boldsymbol{\epsilon}_{k-1}^j + O(\tau^2)\big) + \tau\triangle\boldsymbol{\epsilon}_k^j + O(\tau^2) \\
&= \beta^2\boldsymbol{e}_{k-1}^j + \beta\tau\triangle\boldsymbol{\epsilon}_{k-1}^j + \tau\triangle\boldsymbol{\epsilon}_k^j + \beta O(\tau^2) + O(\tau^2) \\
&= \beta^2\boldsymbol{e}_{k-1}^j + \beta^1\tau\triangle\boldsymbol{\epsilon}_{k-1}^j + \beta^0\tau\triangle\boldsymbol{\epsilon}_k^j + O(\tau^2) \\
&\;\;\vdots \\
&= \beta^{k+1}\boldsymbol{e}_0^j + \beta^{k+1}\boldsymbol{\epsilon}_0^j + \ldots + \beta^0\tau\triangle\boldsymbol{\epsilon}_k^j + O(\tau^2).
\end{aligned}$$

Utilizing the triangle inequality theorem obtains $\triangle\boldsymbol{\epsilon}_k^j \leq |\boldsymbol{\epsilon}_k^j| + |\boldsymbol{\epsilon}_{k-1}^j| \leq 2\boldsymbol{\epsilon}_m^j$. Thus, $\boldsymbol{e}_{k+1}^j$ satisfies

$$\begin{aligned}
\boldsymbol{e}_{k+1}^j &\leq \beta^{k+1}\boldsymbol{e}_0^j + \beta^{k+1}\boldsymbol{\epsilon}_0^j + 2\tau\boldsymbol{\epsilon}_m^j(\lambda^k + \ldots + \lambda^0) + O(\tau^2) \\
&= \beta^{k+1}\boldsymbol{e}_0^j + \beta^{k+1}\boldsymbol{\epsilon}_0^j + 2\tau\boldsymbol{\epsilon}_m^j\frac{1-\beta^{k+1}}{1-\beta} + O(\tau^2).
\end{aligned}$$

Since $0 < \beta < 1$, when $k \to \infty$, it further has

$$\lim_{k\to\infty} \boldsymbol{e}_{k+1}^j = \frac{2\boldsymbol{\epsilon}_m^j}{\alpha\tau} + O(\tau^2). \tag{28}$$

Subsequently, the steady-state residual error can be estimated as

$$\lim_{k\to\infty} ||\boldsymbol{e}_{k+1}||_2 = \frac{2||\boldsymbol{\epsilon}_m||_2}{\alpha\tau} + O(\tau^2). \tag{29}$$

The proof is thus completed. □

IV. SIMULATION VERIFICATON

In this part, numerical simulations are performed to demonstrate the convergence process of the unknown matrix $Z(t)$ and the residual error $||\boldsymbol{e}(t)||_2$. Besides, comparison simulations are performed between the CNRI algorithm (6) and the IINRI algorithm (9), without or with noises, illustrating the higher accuracy and the noise-suppressing property of the IINRI algorithm (9). The coefficient matrixes of the dynamic Sylvester equation are set as

$$M(t) = \begin{bmatrix} \sin(t) & \cos(t) \\ -\cos(t) & \sin(t) \end{bmatrix},$$

$$N(t) = \begin{bmatrix} 0.1\sin(t) & 0 \\ 0 & 0.2\cos(t) \end{bmatrix},$$

and

$$L(t) = \begin{bmatrix} 0.1\sin^2(t) - 1 & -0.2\cos^2(t) \\ 0.1\sin(t)\cos(t) & 0.2\sin(t)\cos(t) - 1 \end{bmatrix}.$$

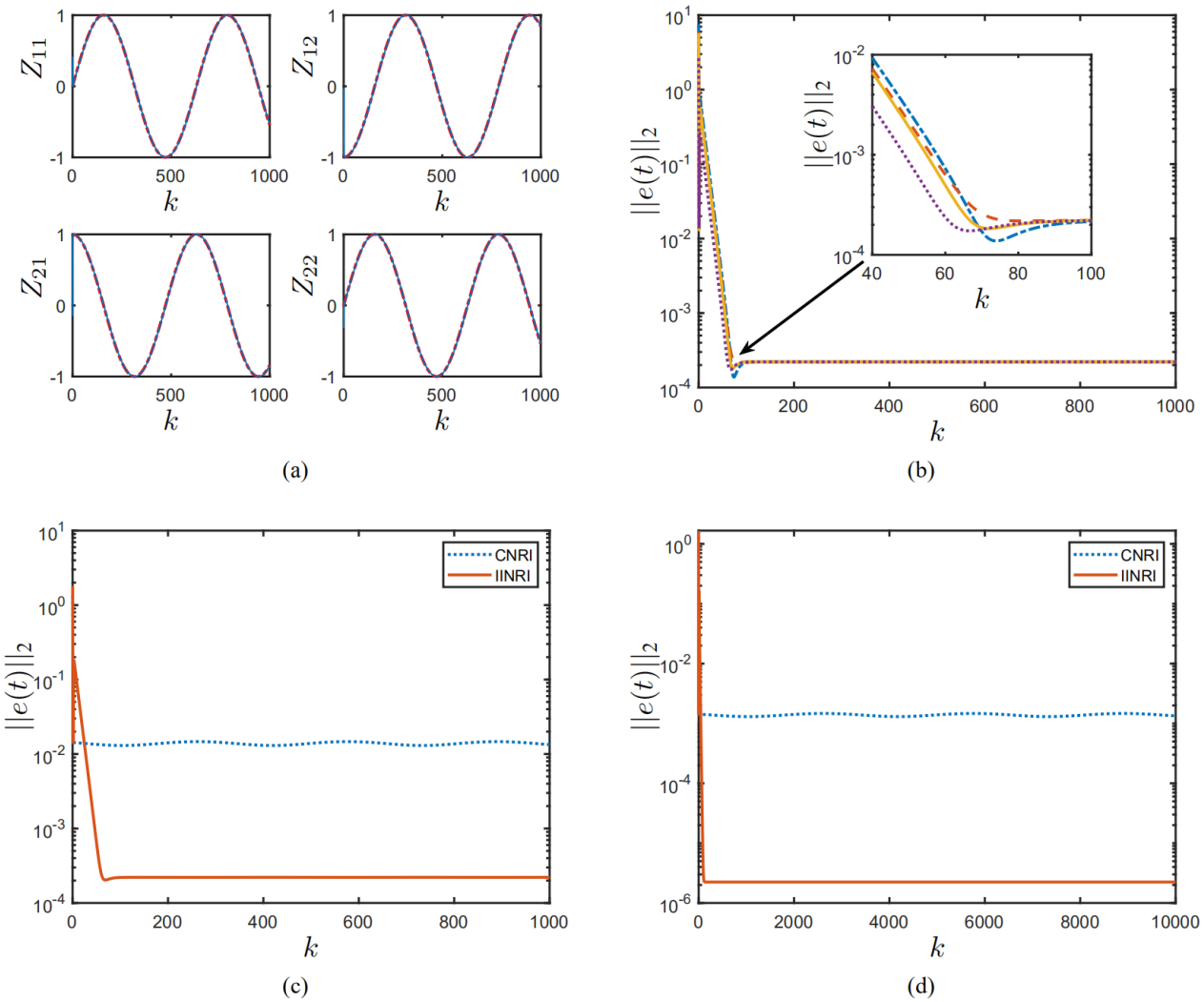

FIGURE 1. Simulation results solved by the IINRI algorithm (9) and the CNRI algorithm (6) without noises. (a) Dynamic of computing and theoretical solution. (b) The residual error synthesized by the IINRI algorithm (9) with four random initial states. (c) Residual error with $\tau = 0.01$ s. (d) Residual error with $\tau = 0.001$ s.

In addition, the Sylvester equation example satisfies the unique solution condition, whose theoretical solution can be expressed as

$$Z(t) = \begin{bmatrix} \sin(t) & -\cos(t) \\ \cos(t) & \sin(t) \end{bmatrix}.$$

A. SIMULATIONS WITHOUT NOISES

Fig. 1(a) illustrates the dynamic of computing solution with the blue solid curve, while the theoretical solution is depicted with the red dash-dot curve. The computing solution can well trace the theoretical solution, which indicates the efficiency of the IINRI algorithm (9). To verify the universal of the IINRI algorithm (9), the simulations are performed from four different random initial states. Subsequently, the residual errors are plotted in Fig. 1(b). All residual errors converge to about 10^{-4}. Moreover, Fig. 1(c) and (d) depict the residual error synthesized by the CNRI algorithm (6) and the IINRI algorithm (9) with $\beta = 0.9$ for different sampling intervals $\tau = 0.01$ and $\tau = 0.001$, respectively. Obviously, the residual error synthesized by the IINRI algorithm (9) changes in an $O(\tau^2)$ manner, which verifies the correctness of the theoretical analyses provided before. Besides, comparing to the CNRI algorithm (6) whose accuracy is $O(\tau)$, the IINRI algorithm (9) possesses higher accuracy indicating its superiority.

B. SIMULATIONS WITH VARIOUS NOISES

For the constant noise, Fig. 2(a) and (b) show the residual error with the sampling interval $\tau = 0.01$ and $\alpha = 10^3$ under different constant-noises $\epsilon = 1$ and $\epsilon = 10$ respectively. Besides, as the theoretical analyses indicate, the values of residual error synthesized by the IINRI algorithm (9) are almost the same as in Fig. 2(a) and (b). Thus, the IINRI algorithm (9) can suppress the constant noise

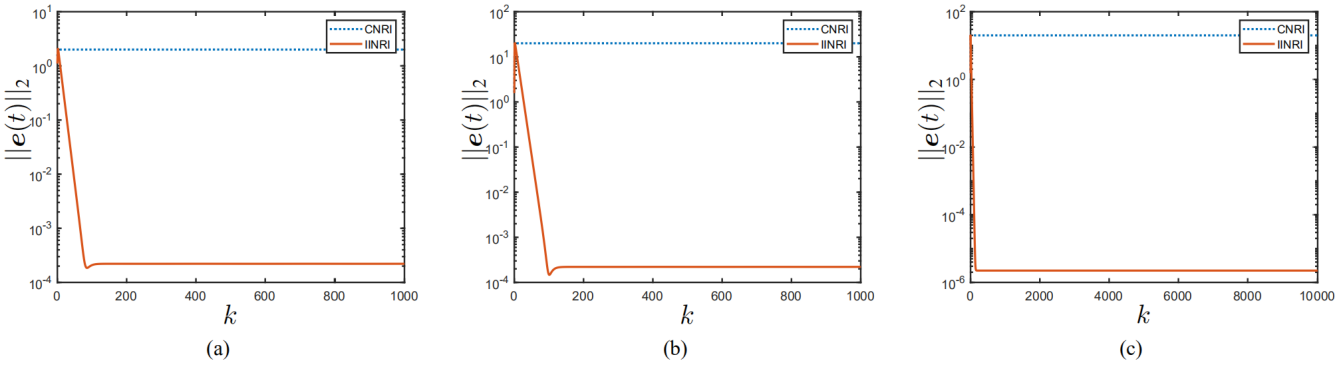

FIGURE 2. Simulation results solved by the IINRI algorithm (9) and the CNRI algorithm (6) with constant noises. (a) Residual error with $\tau = 0.01$ s and $\epsilon = 1$. (b) Residual error with $\tau = 0.01$ s and $\epsilon = 10$. (c) Residual error with $\tau = 0.001$ s and $\epsilon = 10$.

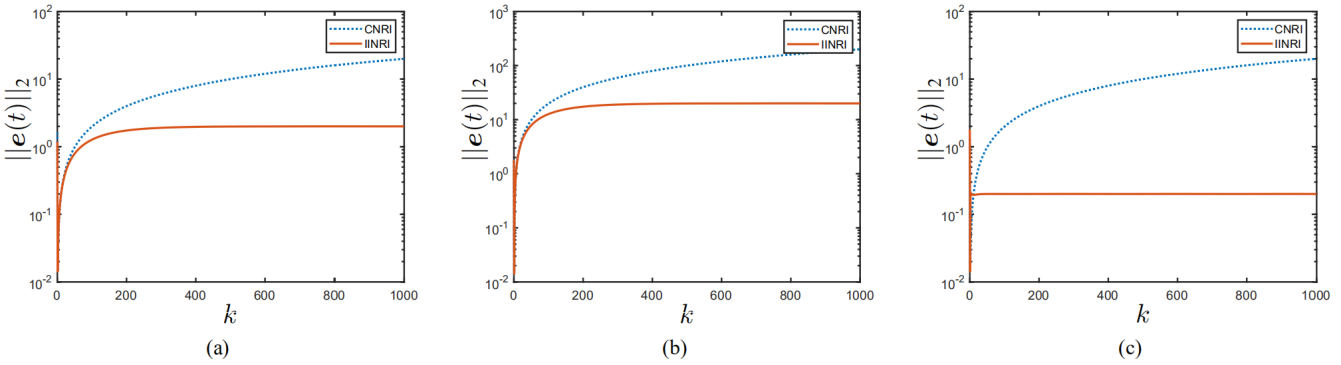

FIGURE 3. Residual error synthesized by the IINRI algorithm (9) and the CNRI algorithm (6) under linear noise perturbation. (a) Residual error with $\tau = 0.01$ s, $\alpha = 100$ and $\gamma = 1$. (b) Residual error with $\tau = 0.01$ s, $\alpha = 100$ and $\gamma = 10$. (c) Residual error with $\tau = 0.01$ s, $\alpha = 1000$ and $\gamma = 1$.

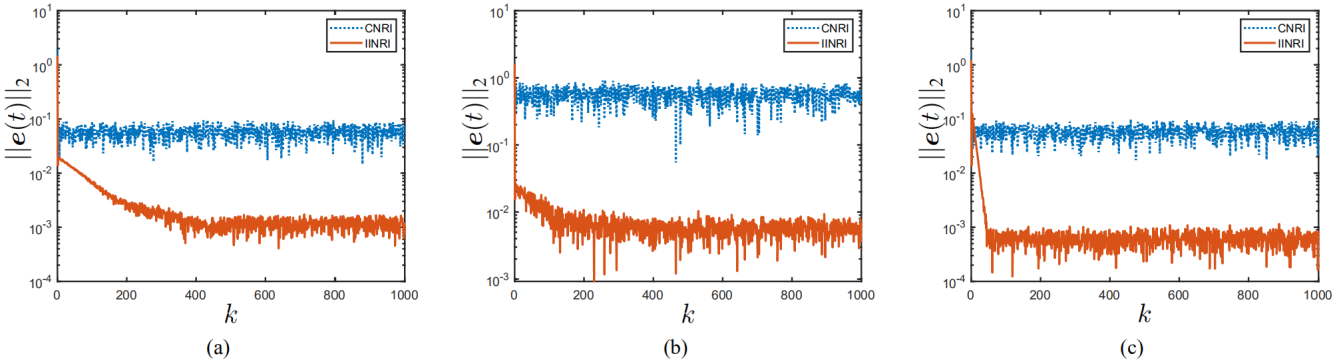

FIGURE 4. Residual error synthesized by the IINRI algorithm the (9) and the CNRI algorithm (6) under bounded random noise perturbation. (a) Residual error with $\tau = 0.01$ s, $\alpha = 100$ and $\epsilon_m = 0.05$. (b) Residual error with $\tau = 0.01$ s, $\alpha = 100$ and $\epsilon_m = 0.5$. (c) Residual error with $\tau = 0.01$ s, $\alpha = 1000$ and $\epsilon_m = 0.05$.

regardless of its value. However, the steady-state residual error synthesized by the CNRI algorithm (6) is proportional to the value of the constant noise. Thus, the performance of the CNRI algorithm (6) can be degraded by the constant noise. Moreover, as shown in Fig. 2(a) and (c), the residual error satisfies changing in an $O(\tau^2)$ manner, which verifies Theorem 2.

With the linear-noise perturbation, as Fig. 3 evidence, the IINRI algorithm (9) is of strong robustness and the residual error would converge to a stable state while residual error synthesized by the CNRI algorithm (6) is divergent. Among Fig. 3, Fig. 3(a) illustrates the convergence of residual error with linear noise $\boldsymbol{\epsilon} = k\tau$ and $\alpha = 100$. From Fig. 3(a) to (b), the slope of the linear noise increases from 1 to 10, the steady-state error of the IINRI algorithm (9) is ten times larger than before. Fortunately, increasing α can suppress the noise. As depicted in Fig. 3(c), by increasing α, the steady-state residual error can be suppressed efficiently.

Finally, the robustness of the IINRI algorithm (9) against the bounded random noise is investigated. Fig. 4(a) and (b) demonstrate the performance with bounded random noises $\epsilon \in [-0.05, 0.05]$ and $\epsilon \in [-0.5, 0.5]$. With a larger random noise boundary, the accuracy of the IINRI algorithm (9) would degrade. As illustrated in Fig. 4(c), the convergence performance of the IINRI algorithm (9) can be improved by increasing α and the accuracy can reach to 10^{-3}.

V. CONCLUSION

This paper has proposed an IINRI algorithm to solve the dynamic Sylvester equation by inserting the integration feedback of the residual error. According to the theoretical analyses and simulation results, the IINRI algorithm is of the strong robustness and high accuracy under various noise perturbation. Especially for the constant noise, the noise effect can be eliminated no matter how large the constant noise is. Regarding the linear noise and the bounded random noise, the IINRI algorithm is of convergence and higher accuracy compare to the CNRI algorithm. Thus, the IINRI algorithm is a superior and powerful method to solve the dynamic Sylvester equation, especially in the noisy working condition. What's more, solving the dynamic Sylvester equation is transformed to a zeroing finding problem in this paper, which indicates that the proposed IINRI algorithm is a potential approach for solving other zeroing finding problems e.g. optimization problem, nonlinear equation and other matrix equations, which can be the future directions of the IINRI algorithm.

REFERENCES

[1] A. Varga, "Robust pole assignment via Sylvester equation based state feedback parametrization," in *Proc. IEEE Int. Symp. Comput.-Aided Control Syst. Design (CACSD)*, Nov. 2002, pp. 13–18.
[2] Y.-D. Liu, D.-W. Zhang, L.-M. Wang, and D.-K. Gu, "Parametric control to second-order quasi-linear systems based on dynamic compensator and multi-objective optimization," *IEEE Access*, vol. 7, pp. 67287–67304, 2019.
[3] H. C. Lee and J. W. Choi, "Linear time-varying eigenstructure assignment with flight control application," *IEEE Trans. Aerosp. Electron. Syst.*, vol. 40, no. 1, pp. 145–157, Jan. 2004.
[4] Q. Wei, N. Dobigeon, and J.-Y. Tourneret, "Fast fusion of multi-band images based on solving a Sylvester equation," *IEEE Trans. Image Process.*, vol. 24, no. 11, pp. 4109–4121, Nov. 2015.
[5] L. Fang, N. He, S. Li, P. Ghamisi, and J. A. Benediktsson, "Extinction profiles fusion for hyperspectral images classification," *IEEE Trans. Geosci. Remote Sens.*, vol. 56, no. 3, pp. 1803–1815, Mar. 2018.
[6] Y. Yankelevsky and M. Elad, "Dual graph regularized dictionary learning," *IEEE Trans. Signal Inf. Process. Netw.*, vol. 2, no. 4, pp. 611–624, Dec. 2016.
[7] Q. Wei, N. Dobigeon, J.-Y. Tourneret, J. Bioucas-Dias, and S. Godsill, "R-FUSE: Robust fast fusion of multiband images based on solving a Sylvester equation," *IEEE Signal Process. Lett.*, vol. 23, no. 11, pp. 1632–1636, Nov. 2016.
[8] M. Darouach, "Solution to Sylvester equation associated to linear descriptor systems," *Syst. Control Lett.*, vol. 55, no. 10, pp. 835–838, Oct. 2006.
[9] Z. Tian, M. Tian, C. Gu, and X. Hao, "An accelerated AC based iterative algorithm for solving Sylvester matrix equations," *Filomat*, vol. 31, no. 8, pp. 2381–2390, 2017.
[10] X. Wang, W.-W. Li, and L.-Z. Mao, "On positive-definite and skew-Hermitian splitting iteration methods for continuous Sylvester equation $AX + XB = C$," *Comput. Math. Appl.*, vol. 66, no. 11, pp. 2352–2361, Dec. 2013.
[11] Y.-J. Xie and C.-F. Ma, "The accelerated gradient based iterative algorithm for solving a class of generalized Sylvester-transpose matrix equation," *Appl. Math. Comput.*, vol. 273, pp. 1257–1269, Jan. 2016.
[12] H. Zhang and H. Yin, "Conjugate gradient least squares algorithm for solving the generalized coupled Sylvester matrix equations," *Comput. Math. Appl.*, vol. 73, no. 12, pp. 2529–2547, Jun. 2017.
[13] W. Zhang and D. Zhou, "Coupled iterative algorithms based on optimisation for solving Sylvester matrix equations," *IET Control Theory Appl.*, vol. 13, no. 4, pp. 584–593, Mar. 2019.
[14] N. A. Zadeh, A. Tajaddini, and G. Wu, "Weighted and deflated global GMRES algorithms for solving large Sylvester matrix equations," *Numer. Algorithms*, vol. 82, no. 1, pp. 155–181, Sep. 2019.
[15] S. Liao, J. Liu, X. Xiao, D. Fu, G. Wang, and L. Jin, "Modified gradient neural networks for solving the time-varying Sylvester equation with adaptive coefficients and elimination of matrix inversion," *Neurocomputing*, vol. 379, pp. 1–11, Feb. 2020.
[16] L. Ding, L. Xiao, K. Zhou, Y. Lan, Y. Zhang, and J. Li, "An improved complex-valued recurrent neural network model for time-varying complex-valued Sylvester equation," *IEEE Access*, vol. 7, pp. 19291–19302, 2019.
[17] Z. Zhang, L. Zheng, J. Weng, Y. Mao, W. Lu, and L. Xiao, "A new varying-parameter recurrent neural-network for online solution of time-varying Sylvester equation," *IEEE Trans. Cybern.*, vol. 48, no. 11, pp. 3135–3148, Nov. 2018.
[18] L. Xiao, Z. Zhang, Z. Zhang, W. Li, and S. Li, "Design, verification and robotic application of a novel recurrent neural network for computing dynamic Sylvester equation," *Neural Netw.*, vol. 105, pp. 185–196, Sep. 2018.
[19] Z. Jian, L. Xiao, J. Dai, Z. Tang, and C. Liu, "Design and analysis of new zeroing neural network models with improved finite-time convergence for time-varying reciprocal of complex matrix," *IEEE Trans Ind. Informat.*, to be published, doi: 10.1109/TII.2019.2941750.
[20] J. Jin, L. Xiao, M. Lu, and J. Li, "Design and analysis of two FTRNN models with application to time-varying Sylvester equation," *IEEE Access*, vol. 7, pp. 58945–58950, 2019.
[21] L. Xiao, "A finite-time recurrent neural network for solving online time-varying Sylvester matrix equation based on a new evolution formula," *Nonlinear Dyn.*, vol. 90, no. 3, pp. 1581–1591, Nov. 2017.
[22] J. Yan, X. Xiao, H. Li, J. Zhang, J. Yan, and M. Liu, "Noise-tolerant zeroing neural network for solving non-stationary Lyapunov equation," *IEEE Access*, vol. 7, pp. 41517–41524, 2019.
[23] H. Lu, L. Jin, X. Luo, B. Liao, D. Guo, and L. Xiao, "RNN for solving perturbed time-varying underdetermined linear system with double bound limits on residual errors and state variables," *IEEE Trans Ind. Informat.*, vol. 15, no. 11, pp. 5931–5942, Nov. 2019.
[24] Z. Xie, L. Jin, X. Du, X. Xiao, H. Li, and S. Li, "On generalized RMP scheme for redundant robot manipulators aided with dynamic neural networks and nonconvex bound constraints," *IEEE Trans Ind. Informat.*, vol. 15, no. 9, pp. 5172–5181, Sep. 2019.
[25] L. Jin, J. Yan, X. Du, X. Xiao, and D. Fu, "RNN for solving time-variant generalized Sylvester equation with applications to robots and acoustic source localization," *IEEE Trans Ind. Informat.*, to be published, doi: 10.1109/TII.2020.2964817.
[26] Y. Qi, L. Jin, H. Li, Y. Li, and M. Liu, "Discrete computational neural dynamics models for solving time-dependent Sylvester equations with applications to robotics and MIMO systems," *IEEE Trans Ind. Informat.*, to be published, doi: 10.1109/TII.2020.2966544.
[27] M. Mao, J. Li, L. Jin, S. Li, and Y. Zhang, "Enhanced discrete-time Zhang neural network for time-variant matrix inversion in the presence of bias noises," *Neurocomputing*, vol. 207, pp. 220–230, Sep. 2016.
[28] L. Jin, Y. Zhang, and S. Li, "Integration-enhanced Zhang neural network for real-time-varying matrix inversion in the presence of various kinds of noises," *IEEE Trans. Neural Netw. Learn. Syst.*, vol. 27, no. 12, pp. 2615–2627, Dec. 2016.
[29] G. Wang, C. Li, Y. Zhu, J. Zhong, Y. Lu, C.-H. Chan, and R. P. Martins, "missing-code-occurrence probability calibration technique for DAC nonlinearity with supply and reference circuit analysis in a SAR ADC," *IEEE Trans. Circuits Syst. I, Reg. Papers*, vol. 65, no. 11, pp. 3707–3719, Nov. 2018.
[30] D. H. Dini and D. P. Mandic, "Class of widely linear complex Kalman filters," *IEEE Trans. Neural Netw. Learn. Syst.*, vol. 23, no. 5, pp. 775–786, May 2012.

[31] D. V. Prokhorov, "Training recurrent neurocontrollers for robustness with derivative-free Kalman filter," *IEEE Trans. Neural Netw.*, vol. 17, no. 6, pp. 1606–1616, Nov. 2006.
[32] J. Kannala and S. S. Brandt, "A generic camera model and calibration method for conventional, wide-angle, and fish-eye lenses," *IEEE Trans. Pattern Anal. Mach. Intell.*, vol. 28, no. 8, pp. 1335–1340, Aug. 2006.
[33] S. Wang, S. Tan, Y. Gao, Q. Liu, L. Ying, T. Xiao, Y. Liu, X. Liu, H. Zheng, and D. Liang, "Learning joint-sparse codes for calibration-free parallel MR imaging," *IEEE Trans. Med. Imag.*, vol. 37, no. 1, pp. 251–261, Jan. 2018.
[34] L. Jin, Y. Zhang, S. Li, and Y. Zhang, "Noise-tolerant ZNN models for solving time-varying zero-finding problems: A control-theoretic approach," *IEEE Trans. Autom. Control*, vol. 62, no. 2, pp. 992–997, Feb. 2017.
[35] L. Jin, S. Li, and B. Hu, "RNN models for dynamic matrix inversion: A control-theoretical perspective," *IEEE Trans Ind. Informat.*, vol. 14, no. 1, pp. 189–199, Jan. 2018.
[36] L. Jin and Y. Zhang, "Continuous and discrete Zhang dynamics for real-time varying nonlinear optimization," *Numer. Algorithms*, vol. 73, no. 1, pp. 115–140, Sep. 2016.

GUANCHENG WANG received the B.E. degree in automation from Sun Yat-sen University, Guangzhou, in 2014, and the M.S. degree in electrical and computer engineering from the University of Macau, Macao, China, in 2017. He works with the School of Electronics and Information Engineering, Guangdong Ocean University, Zhanjiang, China. His current research interests include neural networks, signal processing, and analog and mixed-signal circuit designs.

HAOEN HUANG received the B.E. degree in electrical engineering and automation from Guangdong Ocean University, Zhanjiang, China, in 2019, where he is currently pursuing the M.Agr. degree in agricultural engineering and information technology with the School of Electronics and Information Engineering. His current research interests include Newton algorithm, neural networks, and robotics.

JINGKUN YAN received the B.E. degree in automation from the Beijing Institute of Technology, Beijing, China, in 2018. She is currently pursuing the M.E. degree in communication and information systems with the School of Information Science and Engineering, Lanzhou University, Lanzhou, China. Her research interests include neural networks and robotics.

YIHANG CHENG is currently pursuing the B.E. degree with the School of Electronic and Information Engineering, Guangdong Ocean University, Zhanjiang, China. His current research interests include neural networks and ocean color remote sensing.

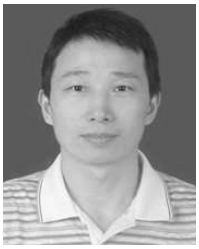

DONGYANG FU received the Ph.D. degree from the South China Sea Institute of Oceanology, Chinese Academy of Sciences. He was a Postdoctoral Researcher with the State Key Laboratory of Satellite Ocean Environment Dynamics, Second Institute of Oceanography, State Oceanic Administration, Guangzhou, China. He is currently a Professor with the School of Electronics and Information Engineering, Guangdong Ocean University, Zhanjiang, China. His current research interests include ocean color remote sensing and its application, remote sensing in offshore water quality, response of upper ocean to typhoon, and neural networks.